frontiers | Frontiers in Energy Research

TYPE Original Research
PUBLISHED 19 January 2024
DOI 10.3389/fenrg.2024.1333686

OPEN ACCESS

EDITED BY
Xiaojin Zheng,
Princeton University, United States

REVIEWED BY
Jianwei Cheng,
China University of Mining and Technology, China
Shixiang Tian,
Guizhou University, China

*CORRESPONDENCE
Yunpei Liang,
liangyunpei@126.com
Wanjie Sun,
sunwanjie@outlook.com

RECEIVED 05 November 2023
ACCEPTED 04 January 2024
PUBLISHED 19 January 2024

CITATION
Liang Y, Sun W, Wu Z, Mao S and Ran Q (2024), Effect of disturbed coal pore structure on gas adsorption characteristics: mercury intrusion porosimetry.
Front. Energy Res. 12:1333686.
doi: 10.3389/fenrg.2024.1333686

Effect of disturbed coal pore structure on gas adsorption characteristics: mercury intrusion porosimetry

Yunpei Liang[1,2]*, Wanjie Sun[1,2]*, Zhaopeng Wu[1,2], Shuren Mao[1,2] and Qican Ran[1,2]

[1]State Key Laboratory of Coal Mine Disaster Dynamics and Control, Chongqing University, Chongqing, China, [2]School of Resources and Safety Engineering, Chongqing University, Chongqing, China

Studying pore structures of disturbed coal and their influences on adsorption characteristics is conducive to in-depth understanding of occurrence and migration of gas in reservoirs in areas prone to coal and gas outbursts. A mercury porosimeter and a high-pressure gas adsorption instrument were separately used to investigate pore structures and measure adsorption characteristics of disturbed coal and undisturbed coal in Ningtiaota Coal Mine and Xigu Coal Mine (Shaanxi Province, China). In addition, pore structures and gas adsorption characteristics of coal samples were studied. The Menger's sponge model was adopted to calculate fractal dimensions of coal samples, to estimate influences of pore structures and fractal features on the gas adsorption characteristics of disturbed and undisturbed coal. Results show that the pore volume of undisturbed coal is mainly contributed by micropores and transitional pores, while that of disturbed coal arises mainly from macropores and mesopores. Micropores and transitional pores account for large proportions of the specific surface area of pores in both disturbed and undisturbed coal. The adsorption isotherms of disturbed and undisturbed coal conform to the Langmuir equation and tectonism increases the limiting adsorption quantity of coal. The fractal dimensions D_1 of the four types of coal samples in the experiments are in the range of 2.7617–2.9961, while the fractal dimensions D_1 and D_2 of disturbed coal are both larger than those of undisturbed coal, indicating that disturbed coal is more likely to collapse under high pressure. The total pore volume, total specific surface area of pores, and fractal dimensions are positively correlated with the adsorption constant *a*, while they have U-shaped correlations with the adsorption constant *b* of coal samples. The adsorption constant *a* of disturbed coal is always greater than that of undisturbed coal, while no obvious trend is observed between the adsorption constant *b* and tectonism. The research results can provide theoretical basis for further study of gas occurrence in disturbed coal seams.

KEYWORDS

disturbed coal, coalbed methane, pore structures, mercury intrusion porosimetry, adsorption characteristics

1 Introduction

Coal reservoirs in China mainly occur at depth; because the geological and coal mining conditions are characterized by high crustal stress, high geothermal temperature, high gas content, and low permeability, gas accidents such as coal and gas outbursts occur frequently (Lu et al., 2015; Wang and Du, 2020; Zhao et al., 2023a; Zou et al., 2023a). The development of gas accidents is generally related to the complex geological structures of reservoirs, which directly or indirectly affect the burial depth, gas occurrence, and gas permeability of surrounding rocks of coal seams (Huang et a.,2023; Tan et al., 2021; Zhao et al., 2023b; Zou et al., 2023b). In fact, the majority of gas accidents happen in the deformation zone of geological structures, and geological structures are important in controlling such outbursts (Zhai et al., 2016; Zhang et al., 2020; Tan et al., 2023). A soft structural coal belt with a certain thickness is generally developed in areas prone to outbursts. After the long geotectonic evolution, the primary structures of coal experience different extents of embrittlement, fracture, deformation, and superimposed damage, and the resulting coal is porous, has a low strength and low permeability (Hou et al., 2012; Ran, Liang, Zou, and Hong et al., 2023; An and Cheng, 2014; Ye et al., 2023). The pore structure characteristics of such coal have become one of the important foci of research into techniques for the control of gas disasters in coal mines (Ran, Liang, Zou, and Zhang et al., 2023; Wang et al., 2019; Xu et al., 2019).

In recent years, numerous researchers have investigated the mechanism of formation (Jiang et al., 2010; Cao et al., 2020), reservoir property (Pan et al., 2012; Dong et al., 2018), pore structure (Li et al., 2015), and adsorption characteristic (Li et al., 2019; Sun et al., 2021; Yang et al., 2021) of disturbed coal. Based on mercury intrusion porosimetry, Qu et al. (2010) compared and studied the pore structures and compressibility of different types of disturbed coal and found that tectonism mainly increases the volume of pores with a diameter exceeding 100 nm. In addition, the more intense the tectonism, the larger the number of open pores and the stronger the connectivity of pore networks. The compressibility reduces with the increasing intensity of tectonism. The differences in porosity and pore compressibility are influenced by tectonism to a significant extent. Dong et al. (2020) calculated pore tortuosity of disturbed coal under different pressures. They found that the pore tortuosity increases with increasing pressure and the pore tortuosity of disturbed coal is always higher than that of undisturbed coal. Wang et al. confirmed that the gas adsorption capacity of disturbed coal is positively correlated with the metamorphic grade of the coal, and therefore believed that the extent of development of pore structures plays an important role. Zhao et al. (2020) studied the influences of the mass ratio of disturbed coal on the amount of gas adsorption of coal and the initial speed of gas diffusion and stated that the gas adsorption increases with the increasing proportion (by mass) of disturbed coal. During gas adsorption, the hardness (Sun et al., 2020; Ullah et al., 2022), structural classification (Li et al., 2015; Wang et al., 2020), metamorphic grade (Meng and Li, 2018; Ren et al., 2022), and water content (Liu et al., 2022) of coal all exert different influences on the gas adsorption.

Existing research approaches for pore structures in coal mainly include mercury intrusion porosimetry (Okolo et al., 2015; Yu et al., 2018), magnetic resonance imaging (Zhao et al., 2017), scanning electron microscopy (Kutchko et al., 2013), N_2/CO_2 adsorption (Nie et al., 2015; Chu et al., 2024), and transmission electron microscopy (Lee et al., 2006). Agbabiaka et al. (2013) studied the fractal features of spherical pores using scanning electron microscopy and a small-angle X-ray scattering method. Jia et al. (2022) and Lin et al. (2020) explored the porosity and pore size of coal at different metamorphic grades by conducting mercury injection and low-temperature liquid nitrogen adsorption experiments. By using scanning electron microscopy and low-pressure N_2/CO_2 adsorption, Mangi et al. (2020) systematically evaluated influences of pore size distribution and fractal dimension on gas adsorption and desorption quantities. Wang et al. (2021) conducted low-temperature liquid nitrogen adsorption experiments to explore adsorption characteristics of micropores in coal at low temperature and low pressure. In the study of coal pore structure, fractal dimension can represent the complexity or roughness of coal pore structure, so as to effectively represent pore characteristics. There are many calculation methods for fractal dimension, includes Menger (Fu et al., 2005; Zhao et al., 2023), Frenkel-Halsey-Hill (Yao et al., 2008; Huang L. K. et al., 2023; Huang L. et al., 2023), BET (Dormant and Adamson, 1972; Lin et al., 2023) and Langmuir (Rigby, 2005; Ji et al., 2023) fractal models, *etc.* Previous research results play a positive role in understanding pore structure characteristics of disturbed coal and studying the gas adsorption characteristics thereof; however, due to the complexity of disturbed coal, research into the influences of pore structures in disturbed coal on gas adsorption should be studied further. The pore structure in coal is an important index representing gas adsorption capacity and rate. Due to the low Protodyakonov coefficient, high initial speed of gas diffusion, and low permeability, disturbed coal seams are found to exhibit complex gas emission behaviors in the mining process and therefore are difficult to treat. Hence, it is necessary to study the difference of disturbed coal and undisturbed coal in pore structures and their influences on the gas adsorption characteristics. Disturbed coal and undisturbed coal in Ningtiaota Coal Mine and Xigu Coal Mine in Shaanxi Province, China were selected, for which mercury injection experiments and gas adsorption experiments were conducted to test microstructures of pores and gas adsorption characteristics. The microstructural characteristics of disturbed coal and their influences on gas adsorption characteristics were studied, to provide a theoretical basis for in-depth research on gas occurrence in disturbed coal seams.

2 Experimental instruments and methods

2.1 Sampling locations and basic parameters

Coal samples used in the experiments were separately obtained from the tectonic regions (faults) and non-tectonic regions of Ningtiaota Coal Mine and Xigu Coal Mine in Shaanxi Province, located in Ordos Basin and the folded zone on its margin. The sampling locations are shown in Figure 1. The disturbed coal is obtained near the structural zone by coring long drilling holes, and the undisturbed coa as a contrast is obtained

FIGURE 1
Sampling locations.

TABLE 1 Industrial analysis results of coal samples.

Sample	M_{ad}/wt%	A_d/wt%	V_{ad}/wt%	FC_{ad}/wt%	f
NT01	2.63	17.19	10.28	69.90	1.62
NT02	2.19	24.38	11.73	61.70	0.35
XG01	0.44	19.06	14.86	65.79	0.68
XG02	0.32	18.10	15.57	66.12	0.28

Notes: M_{ad}, moisture, air-drying basis; A_{ad}, ash yield, air-drying basis; V_{ad}, volatile, air-drying basis; FC_{ad}, fixed carbon content, air-drying basis; f, firmness coefficient.

from the intact coal wall without structure. The coal samples were drilled, then sealed, and taken to the laboratory. The undisturbed coal in Ningtiaota Coal Mine, disturbed coal in Ningtiaota Coal Mine, undisturbed coal in Xigu Coal Mine, and disturbed coal in Xigu Coal Mine were separately labelled NT01, NT02, XG01, and XG02.

Basic industrial parameters of coal samples were tested using a coal quality industrial analyzer (Table 1). The two types of coal samples both belonged to bitumite at a low metamorphic grade and contained a low water content (0.32%–2.63%). The firmness coefficient of the coal samples was tested. The firmness coefficients f of the two types of disturbed coal are obviously lower (by 78.39% and 26.82%) compared with those of the undisturbed coal, which indicates that coal subjected to tectonism softened, became more prone to fracture, and its strength decreased.

2.2 Pore tests

An Auto Pore IV 9510 mercury porosimeter was adopted to perform mercury injection experiments (Figure 2). The high pressure mercury intrusion porosimetry method is the most commonly used method to test the pore structure of coal and shale at present. This method mainly relies on the intrusion of mercury into the pores of coal body under high pressure. The pore diameter, pore specific surface area and porosity of coal body can be calculated by the curve of mercury content as the pressure changes. The range of test pressure and the measurement range of pore size of the instrument were 0–413 MPa and 3 nm to 370 μm, respectively. Coal specimens with particle sizes ranging from 2.8 to 4 mm were selected. After vacuum-drying in an oven at 80°C for 8 h, a coal sample of 5 g was placed in a dilatometer, which was then sealed and put in the low and high-pressure chambers successively to conduct

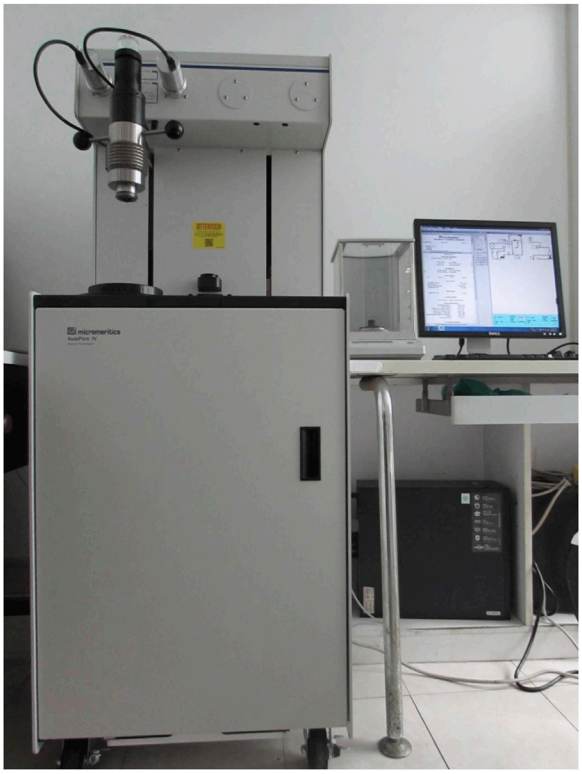

FIGURE 2
Auto Pore IV 9510 mercury porosimeter.

mercury injection experiments. The surface tension of mercury, contact angle of mercury with the sample, and density of the mercury were separately 0.485 N/m, 130°, and 13.5335 g/cm^3.

2.3 Adsorption tests

A self-built automatic high-pressure gas adsorption instrument was used to conduct methane adsorption experiments on coal. The test pressure and the highest test temperature of the instrument were separately 0–20 MPa and 200°C. With high precision, the instrument was able to monitor subtle changes in the adsorption achieved in the initial stage of adsorption (Figure 3). Four types of pulverized coal of 6–7 g with the particle size ranging from 0.18 to 0.25 mm could be prepared. Before experiments, the pulverized coal was degassed under vacuum for 6 h. Thereafter, isothermal adsorption experiments for methane were conducted under an initial adsorption pressure of 5 MPa and a temperature of 30°C, ambient temperature of (25 ± 2) °C, and relative humidity of 30%.

3 Test results and analysis

3.1 Mercury injection and ejection curves

Many experiments on the microstructure of coal reveal that the mercury injection and ejection curves of the coal samples are not overlapped but exhibit a certain hysteresis. The coal samples tested also exhibit differences in pore structure characteristics,

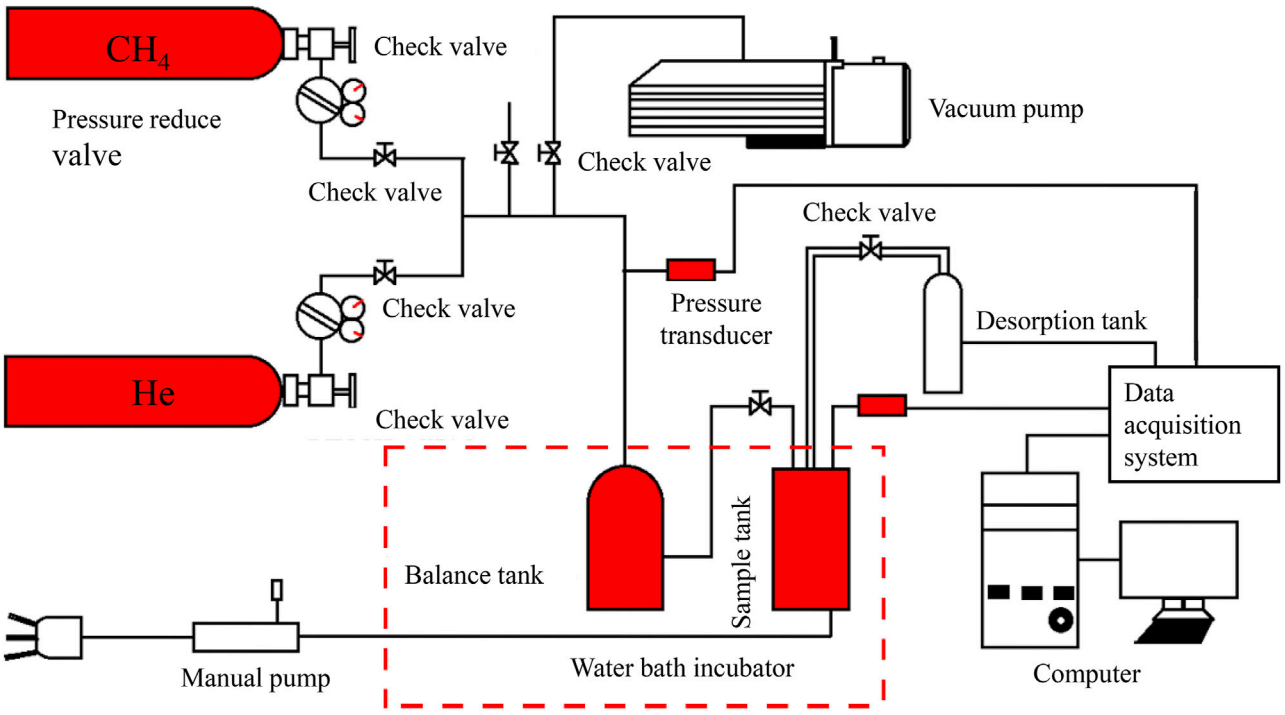

FIGURE 3
High-pressure gas adsorption instrument.

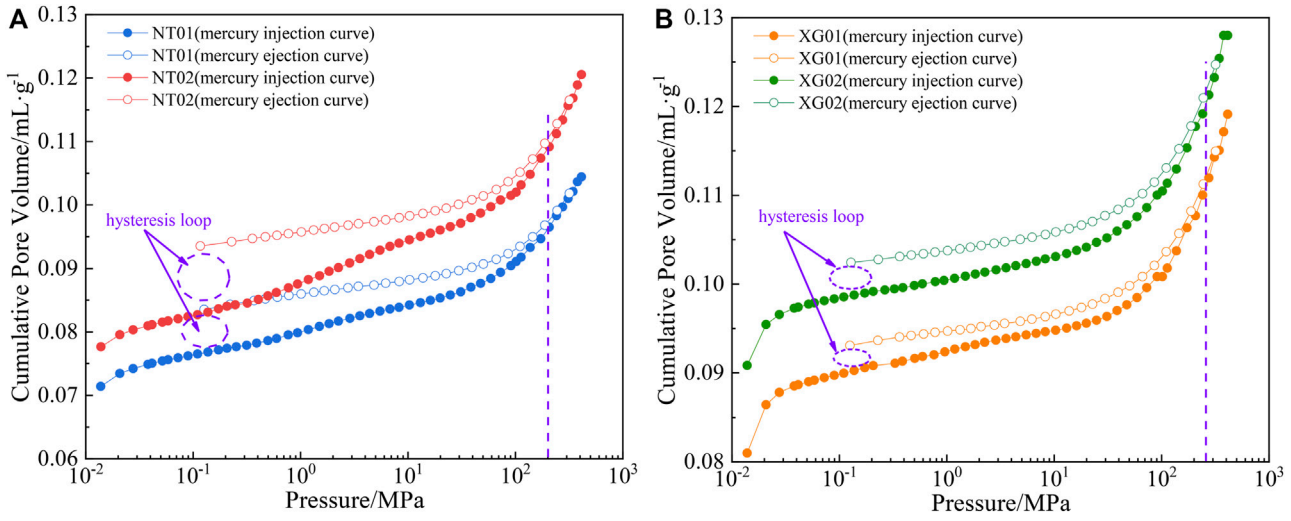

FIGURE 4
Mercury injection and ejection curves of coal samples. **(A)** NT01 and NT02; **(B)** XG01 and XG02.

therefore, the morphological characteristics of pores are commonly analyzed according to hysteresis loops of mercury injection and ejection curves.

According to mercury injection experimental data, mercury injection and ejection curves of each coal sample were drawn, as shown in Figure 4.

The mercury injection curves of coal samples NT01 and NT02 ascend in an inverted S-shape in the low-pressure mercury injection stage, while linearly descend in main sections of the high-pressure mercury ejection stage. The mercury ejection curves start from mercury withdrawal and pressure relief. The difference in pore volume at the same pressure gradually increases with decreasing pressure and the mercury ejection curves begin to depart from mercury injection curves and descend slowly when the pressure is decreased to 200–300 MPa. Under such conditions, the difference in pore volume increases significantly, indicative of a high proportion of open pores in coal samples. The mercury injection and ejection curves of coal samples XG01 and XG02 are both manifest as concave arcs. When the pressure is below 300 MPa, the hysteresis loops are enlarged, which suggests that pores in coal samples are mainly semi-closed and thin-necked, bottle-shaped pores, and there are a certain number of these present as open macropores. Disturbed coal samples taken from the same coal mine show similar forms of mercury injection and ejection curves compared with undisturbed coal, while the hysteresis loops of disturbed coal are larger than those of undisturbed coal. This indicates that pore connectivity of the coal subjected to tectonism is greatly enhanced, which increases the volume available to gas. The result suggests that gas is likely to diffuse during pressure relief in a disturbed coal seam, which explains why a large amount of gas is more likely to escape within a short time when mining disturbed coal seams from the perspective of pores. This is extremely likely to trigger coal and gas outburst accidents, so gas drainage with pressure relief should be mainly performed in the coal mining process.

3.2 Distribution characteristics of pore volume and specific surface area

When using the Mercury Intrusion Porosimetry to study pore structures, the pore classification method proposed by Hodot is generally used (Hodot, 1966). According to the pore diameter, pores can be classified into micropores (<10 nm), transitional pores (10–10^2 nm), mesopores (10^2–10^3 nm), macropores (10^3–10^5 nm), and visible holes and fractures (>10^5 nm).

The pore volume in unit mass of coal is a reference basis for gas storage capacity and extent and severity of failure therein. The distribution of pore volumes in different coal samples is shown in Table 2. The pore volume of undisturbed coal is mainly contributed by micropores and transitional pores: micropores and transitional pores separately account for 55.88% and 31.27% of the total pore volume in sample NT01, while macropores and mesopores are less well developed and separately account for 7.22% and 5.64% of the total volume. Micropores and transitional pores separately account for 34.54% and 53.27% of total pore volume in sample XG01, which also contains a small number of macropores (5.21%) and mesopores (6.98%). This indicates that undisturbed coal exhibits weak tectonic deformation and pores mainly include primary pores. The pore volume in disturbed coal is mainly contributed by macropores and mesopores. Due to brittle deformation of sample XG02, the pore structures change substantially: the volume of macropores and mesopores increases (with proportions of 35.29% and 34.58% separately) while that of micropores and transitional pores are decreased, which separately account for 15.26% and 14.88% of the total volume. Sample NT02 is deformed more than sample XG02 and the proportion of macropores (by volume) increases to a greater extent, accounting for 45.31% of the total pore volume; the proportion (by volume) of mesopores (36.84%) is similar to that in sample XG02, while the volume of micropores and transitional pores further decreases to proportions of 8.17% and 9.68%, respectively.

The distribution of pore volume of coal reveals that the total pore volume of undisturbed coal arises mainly in the form of

TABLE 2 Distribution of pore volume of coal samples.

Coal samples	Total pore volume /$cm^3 \cdot g^{-1}$	Pore volume/$cm^3 \cdot g^{-1}$				Proportion of pore volume/%			
		Macropores	Mesopores	Transitional pores	Micropores	Macropores	Mesopores	Transitional pores	Micropores
NT01	0.1045	0.0075	0.0059	0.0327	0.0584	7.22	5.63	31.27	55.88
NT02	0.1192	0.0540	0.0439	0.0115	0.0097	45.31	36.84	9.68	8.17
XG01	0.1144	0.0059	0.0080	0.0610	0.0395	5.20	6.97	53.28	34.55
XG02	0.1369	0.0483	0.0473	0.0204	0.0209	35.29	34.58	14.88	15.26

TABLE 3 Distribution of specific surface area of pores in coal samples.

Coal samples	Total specific surface area/ $cm^2 \cdot g^{-1}$	Specific surface area of pores/$cm^2 \cdot g^{-1}$				Proportion of specific surface area of pores/%			
		Macropores	Mesopores	Transitional pores	Micropores	Macropores	Mesopores	Transitional pores	Micropores
NT01	11.3462	0.0023	0.0238	1.2401	10.0799	0.02	0.21	10.93	88.84
NT02	15.3471	0.0010	0.2400	2.0219	13.0840	0.01	1.56	13.17	85.25
XG01	14.6394	0.0117	0.0176	1.6733	12.9368	0.08	0.12	11.43	88.37
XG02	15.6609	0.0016	0.0235	1.9686	13.6673	0.01	0.15	12.57	87.27

10.3389/fenrg.2024.1333686

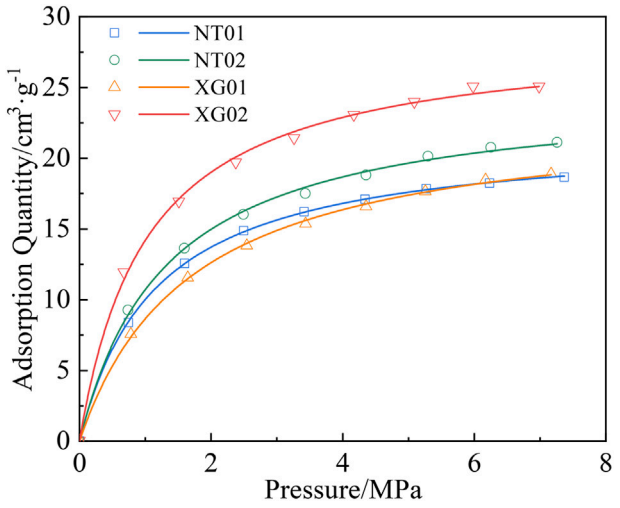

FIGURE 5
Isothermal adsorption curves of coal samples.

micropores and transitional pores, which indicates that undisturbed coal is slightly deformed and pores are mainly dominated by primary pores and a small number of metamorphic pores. In comparison, most pores in disturbed coal are macropores and mesopores. Sample NT02 is more significantly deformed than sample XG02, so the proportion of macropores increases more in sample NT02. This suggests that as the deformation of the coal increases, the proportions of macropores and mesopores also increases, especially macropores, which increase to an even greater extent. Macropores are generated along with fractures in coal, forming the principal channels for gas seepage, so the more numerous the macropores, the more permeable the coal seam.

The specific surface area of pores refers to the internal surface areas of all pores in unit mass of coal. The specific surface area of pores is influenced by the shape of pores, surface defects, and pore structures of coal, and is closely related to the degree of development of pores. The distribution of the specific surface areas of pores in various coal samples is summarized in Table 3. In terms of the total specific surface area of pores in coal samples, disturbed coal is akin to undisturbed coal: micropores and transitional pores account for large proportions by total volume. Therein, micropores account for the largest proportion of the specific surface area (88%), while the proportion of transitional pores is 12%; the proportions of specific surface areas of mesopores and macropores are relatively low, both being below 2%.

3.3 Results of adsorption experiments

Figure 5 illustrates the isothermal adsorption curves of coal samples. During low-pressure adsorption (<3 MPa), the gas adsorption by coal samples increases rapidly with increasing pressure. When the pressure exceeds 3 MPa, the adsorption quantity exhibits slow growth. The Langmuir equation (Eq. 1) (Ezzati, 2020) is used to fit the adsorption curves and the fitting results are summarized in Table 4. The degrees of fitting of adsorption curves of the four types of coal samples all exceed 0.99, which means that the adsorption curves of the four types of coal samples all conform to the Langmuir equation. Under the maximum pressure, the samples are listed in an ascending order as NT01, XG01, NT02, and XG02 according to the saturated adsorption quantities. The gas adsorption quantities of the two types of disturbed coal are both larger than those of their corresponding undisturbed coal samples.

$$Q = \frac{abP}{1 + bP} \tag{1}$$

where P represents pressure (MPa); Q denotes the adsorption quantity under pressure P (cm^3/g); a is an adsorption constant (cm^3/g); b is also an adsorption constant (MPa^{-1}).

The values of adsorption constants a and b physically represent the saturated gas adsorption quantity and adsorption rate of coal, respectively. Based on the PCT adsorption experimental data, the Langmuir equation was adopted to calculate the gas adsorption constants of each coal sample. Analysis results of isothermal adsorption experiments on coal samples were obtained (Table 4). Table 4 indicate that the adsorption constant a of the four types of coal samples is between 21.697 and 28.753. The coal samples are also listed in the same order as that according to the saturated adsorption quantities (also in ascending order) as NT01, XG01, NT02, and XG02. Samples XG02 and XG01 separately have the highest and lowest adsorption constant b, namely, 0.975 and 0.593.

4 Discussion

4.1 Fractal features of pores

The fractal dimension of pores in coal can be used as a measure of the irregularity and roughness of pore surfaces. Menger's model (Eq. 2) more suitable for mercury injection experiments was selected

TABLE 4 Measured adsorption characteristics of coal samples.

Coal samples	Adsorption constants		Fitting curves	R^2
	a	b		
NT01	21.697	0.858	$Q = 18.616P/1 + 0.858P$	0.999
NT02	24.812	0.761	$Q = 18.857P/1 + 0.761P$	0.998
XG01	23.249	0.593	$Q = 13.786P/1 + 0.593P$	0.999
XG02	28.753	0.975	$Q = 28.034P/1 + 0.975P$	0.997

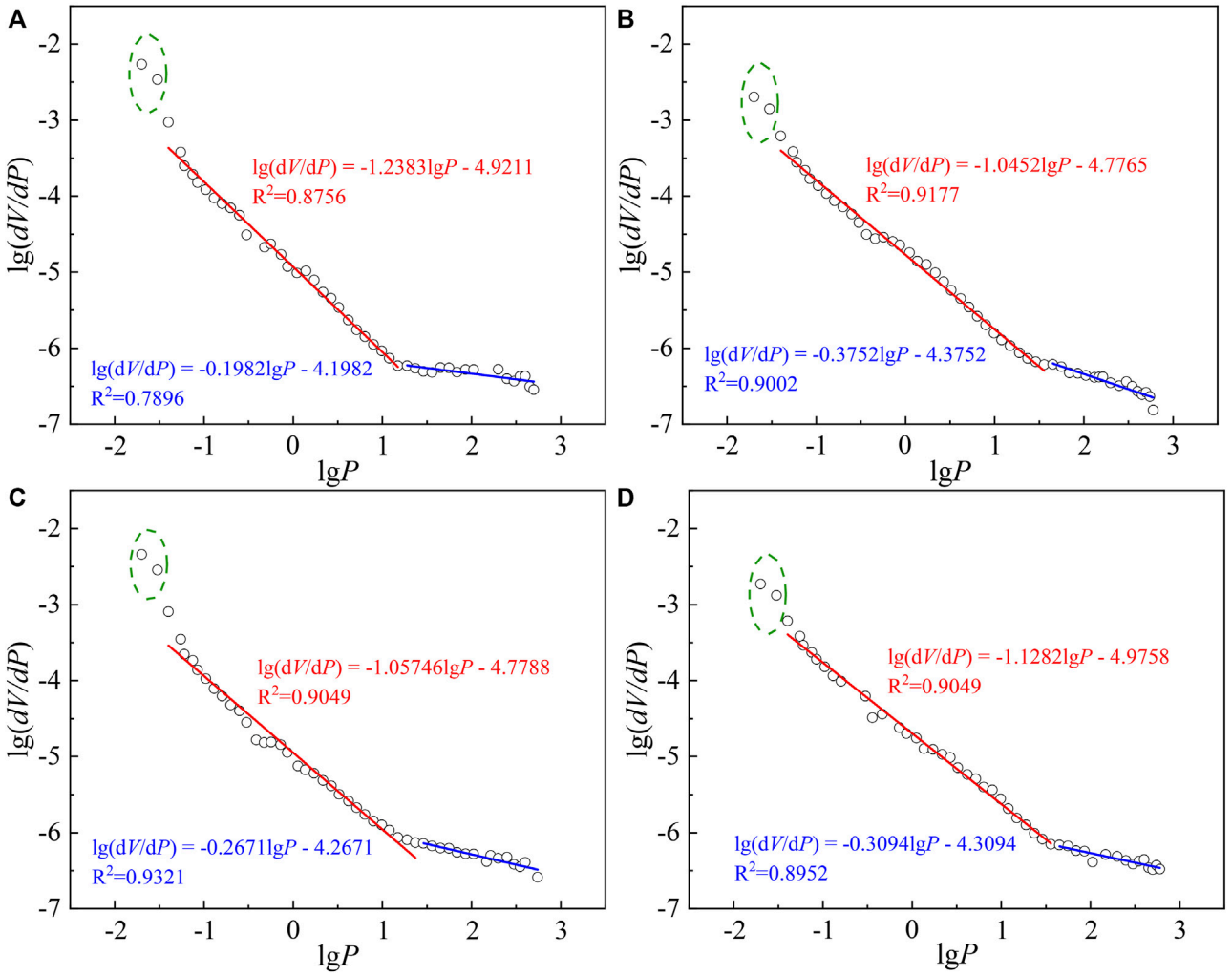

FIGURE 6
Fitted relationship between lg (d*V*/d*P*) and lg*P* of coal samples. **(A)** NT01; **(B)** NT02; **(C)** XG01; **(D)** XG02.

to analyze the experimental results (Han et al., 2020). The fractal dimension calculated following the principle of mercury injection experiments is called the volumetric fractal dimension. In the Menger, porous materials such as coal are assumed to be in the form of a regular cube, leading to:

$$\lg\left[\frac{\mathrm{d}V}{\mathrm{d}P}\right] = \mathrm{A}_2 \lg P \tag{2}$$

where V and P separately represent the mercury intake and pressure in mercury injection experiments; A_2 is the power exponent, which has a linear relationship with the fractal dimension D_2 and its value is the slope of the double logarithmic curves dV/dP and lg P; the fractal dimension is $D_2 = 4 + A_2$.

The pore volume V, applied pressure P, lg (dV/dP), and lg$P$ can be obtained according to experimental data of the four types of coal samples, and then the scatter plots are drawn, as shown in Figure 6, followed by linear fitting. The volumetric fractal dimension of pores can then be calculated according to the slope of the lines. The Fractal dimension fitting and calculation results are shown in Table 5. Combining these data with values of the fractal dimensions of coal specimens, the mercury injection experimental process of coal can be divided into three stages.

1) Pre-injection stage (green circles in Figure 6). Mercury influx first fills the space between coal particles while it does not enter the pores in the coal. The fractal dimension in the stage is generally less than 2. How obvious the stage is related to the particle size of the samples used in the experiments: the smaller the particle size the more obvious the curves in the stage. The coal samples used in the mercury injection experiments have the particle size of 2.8–4 mm, so only several points appear at the start of the curves in mercury injection experiments of the four types of coal samples in the stage, indicating that the stage is not obvious;
2) Injection stage (red fitted lines in Figure 6). Mercury influx fills the pores in the coal under the pressure applied by the instrument. The fractal dimension D_1 in the stage is between 2 and 3. This is a stage in which the fractal dimension can be most effectively and accurately calculated in mercury injection experiments. The larger the absolute

TABLE 5 Fractal dimensions of pores in coal samples.

Coal samples	Injection stage			Post-injection stage		
	Fitting equations	D_2	R^2	Fitting equations	D_3	R^2
NT01	lg (dV/dP) = −1.2383lg$P$–4.9211	2.7617	0.8756	lg (dV/dP) = −0.1982lg$P$–4.1982	3.62125	0.7896
NT02	lg (dV/dP) = −1.0452lg$P$–4.7765	2.9548	0.9177	lg (dV/dP) = −0.3752lg$P$–4.3752	3.71889	0.9002
XG01	lg (dV/dP) = −1.05746lg$P$–4.7788	2.8718	0.9049	lg (dV/dP) = −0.2671lg$P$–4.2671	3.67175	0.9321
XG02	lg (dV/dP) = −1.1282lg$P$–4.9758	2.9961	0.9049	lg (dV/dP) = −0.3094lg$P$–4.3094	3.69491	0.8952

value of the curve slope in the stage, the greater the corresponding volumetric fractal dimension and the more complex the pore structures present in the coal;

3) Post-injection stage (blue fitted lines in Figure 6). In the stage, the increase in the mercury intake is not only because mercury is filled in pores in coal, but also due to the compression effect of mercury on coal. The curves in the stage have a small slope and the calculated fractal dimension D_2 is generally larger than 3. Coal is a porous medium. Due to the compressibility of the coal matrix, when the mercury injection pressure is large, the pore structure of the coal body will be destroyed and collapsed, resulting in the fractal dimension of the high pressure section being greater than 3, and the pore measurement results also have greater errors. The larger the fractal dimension is in the stage, the more easily the coal used in the experiments is compressed. Therefore, the value of the fractal dimension in the stage can be employed to qualitatively describe the compressibility of coal. Among the four types of coal samples selected in the research, sample XG02 has the largest fractal dimension (3.71889), indicating that sample XG02 is most easily compressed.

Therefore, D_1 calculated in the injection stage is adopted as the volumetric fractal dimension to characterize the complexity of pores in coal. The fractal dimension D_2 of experimental coal samples is in the range of 2.7617–2.9961, very approximate to 3, suggesting high complexity of pores in the four types of coal. The fractal dimensions D_1 and D_2 of the two types of disturbed coal are both larger than those of the undisturbed coal. This finding implies that the complexity of pores in the coal subjected to tectonism is increased and the compressibility of pores is also enhanced, so that the coal is more likely to collapse under high pressure.

4.2 Influences of pore structure on adsorption constants

Pores in coal are places for adsorption and free flow of gas. Pore characteristics exert important influences on the gas adsorption and desorption properties of coal. The relationships between pore parameters and adsorption constants (a and b) of undisturbed coal and disturbed coal were estimated. The relationships between total pore volume and adsorption constants are shown in Figure 7; the relationships between the total specific surface area of pores and adsorption constants are illustrated in Figure 8; the relationships between fractal dimensions and adsorption constants are displayed in Figure 9.

Disturbed coal contains highly developed pores. The tectonic stress enhances the pore connectivity and improves the gas adsorption capacity of coal. The void content in coal affects the gas adsorption capacity of coal. As shown in Figure 8A, Figure 9A, the total pore volume and total specific surface area of pores are positively correlated with the adsorption constant a, and the adsorption constant a reflects the maximum amount of gas that can be adsorbed by the coal. The increase in the void content means that coal has a larger potential area over which adsorption can occur and more adsorption sites, so the total amount of gas that can be adsorbed by coal samples with a larger void content also increases. The adsorption constant a of disturbed coal is always greater than that of undisturbed coal, which indicates that tectonism enlarges the volume available to gas storage in disturbed coal specimens.

Figure 8B, Figure 9B show that the total pore volume and total specific surface area of pores of coal have U-shaped correlations with the adsorption constant b of the coal. The adsorption constant b is the pressure under which the coal samples reach the maximum adsorption (by volume). The lack of any significant linear trend in these parameters may arise because of the uncertain changes in pore morphologies due to tectonism. The adsorption constant b is not only related to the void content but also to the pore connectivity.

As illustrated in Figure 9A, the fractal dimensions of coal show strong positive correlations with the adsorption constant a of coal. Compared with undisturbed coal, disturbed coal is found to have a larger fractal dimension of pores, rough internal surfaces, and many pores, so the volume available to gas adsorption is larger and the adsorption thus enhanced. The result indicates that coal samples with different fractal dimensions differ in their gas adsorption capacity. Within a certain range, the larger the volumetric fractal dimension, the stronger the gas adsorption capacity of coal. Figure 9B shows that the fractal dimension of coal has a U-shaped relationship with the adsorption constant b of coal.

5 Conclusion

The pore structures were analyzed and the gas adsorption characteristics were measured for disturbed coal and undisturbed coal in Ningtiaota Coal Mine and Xigu Coal Mine. The pore structure and gas adsorption characteristics of coal samples were investigated, and the Menger sponge model was used to calculate the fractal dimensions of coal. Moreover, influences of pore structures and fractal features on gas adsorption characteristics of disturbed

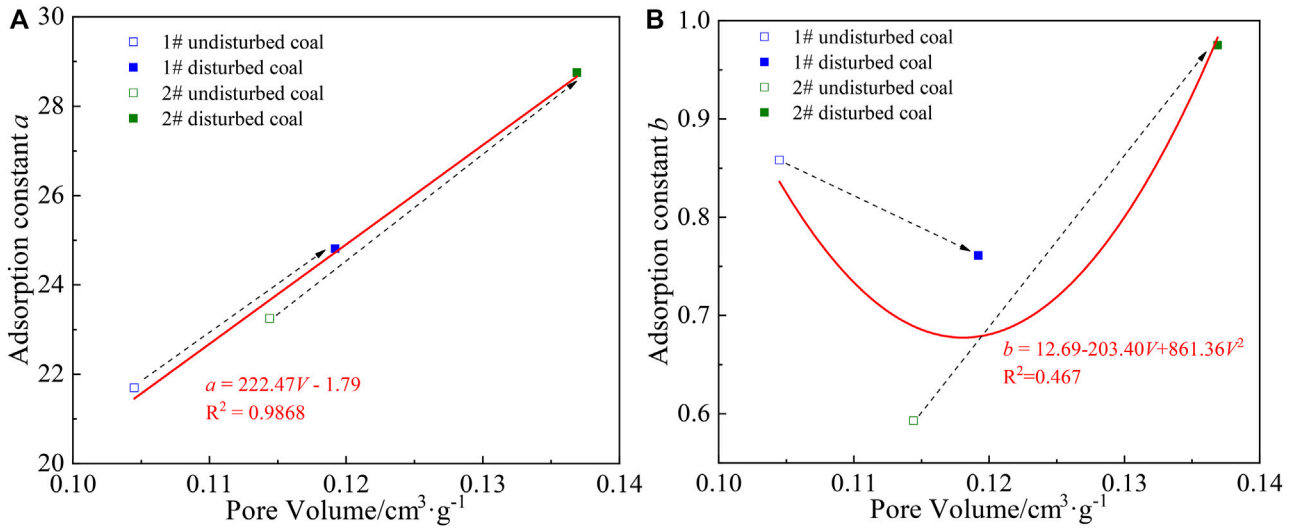

FIGURE 7
Relationships between the total pore volume and adsorption constants. **(A)** Adsorption constant *a*; **(B)** Adsorption constant *b*.

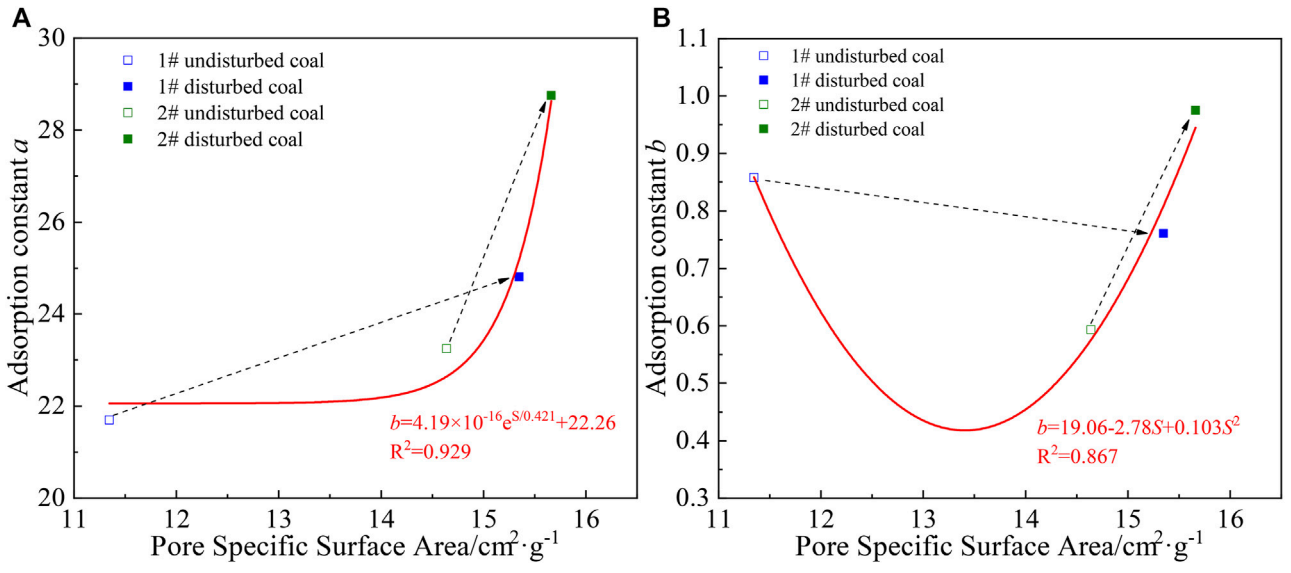

FIGURE 8
Relationships between the total specific surface area of pores and adsorption constants. **(A)** Adsorption constant *a*; **(B)** Adsorption constant *b*.

coal and undisturbed coal were investigated. The results showed that.

1) Mercury intrusion porosimetry was utilized to measure the pore structure characteristics of coal samples. The pore volume of undisturbed coal arises mainly in the forms of micropores and transitional pores, while that of disturbed coal is mainly accounted for by macropores and mesopores. Micropores and transitional pores account for high proportions in specific surface areas of both disturbed coal and undisturbed coal. The results suggest that undisturbed coal is slightly deformed, and pores are dominated by primary pores and a small number of metamorphic pores. After being subjected to structural deformation, the contents of macropores and mesopores increased (especially for macropores, which increase to an even greater extent);
2) The adsorption isotherms of disturbed coal and undisturbed coal conform to the Langmuir equation. The tectonism enhances the limit adsorption quantity of coal by increasing the void content and strengthening the pore connectivity in coal;
3) The mercury injection testing can be divided into the pre-injection, injection, and post-injection stages. The fractal phenomenon is not apparent in the pre-injection stage. The

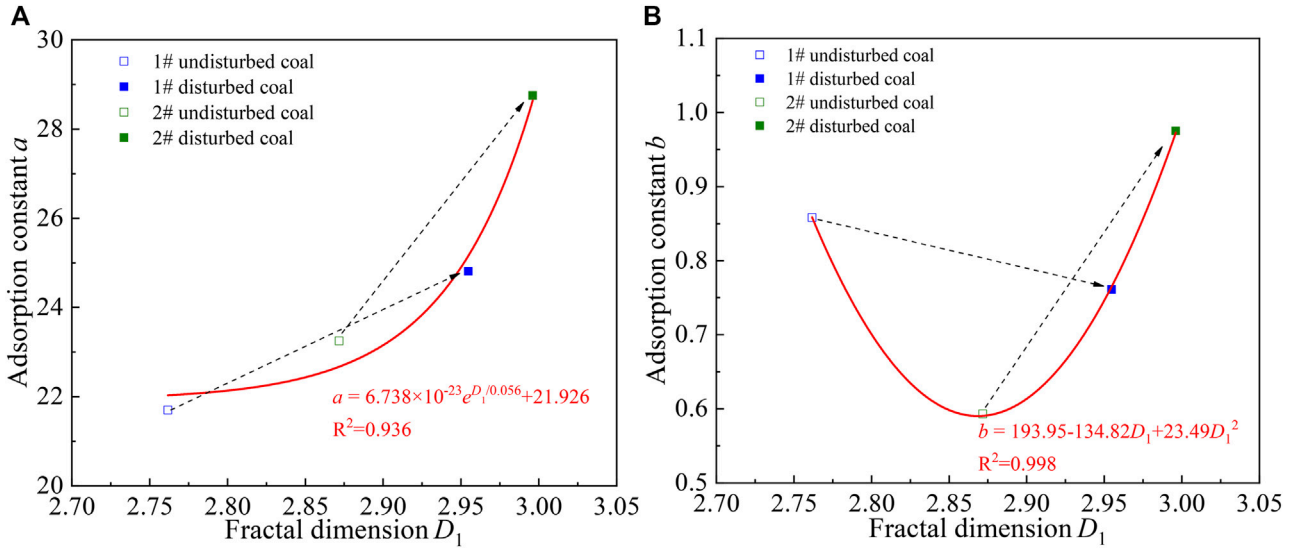

FIGURE 9
Relationships between the fractal dimensions and adsorption constants. **(A)** Adsorption constant *a*; **(B)** Adsorption constant *b*.

fractal dimensions D_1 of the four types of experimental coal samples calculated in the injection stage range between 2.7617 and 2.9961. The fractal dimension calculated in the post-injection stage is always greater than 3. The fractal dimensions D_1 and D_2 of disturbed coal are both greater than those of undisturbed coal. Pores in disturbed coal are more likely to collapse under high pressure;

4) The total pore volume, total specific surface area of pores, and fractal dimensions have positive correlations with the adsorption constant *a* and U-shaped correlations with the adsorption constant *b* of coal. The adsorption constant *a* of disturbed coal is always greater than that of undisturbed coal. This is because the increasing void content due to tectonism means that the coal has a larger potential area over which adsorption can occur and more numerous adsorption sites. As a result, the total gas content that can be adsorbed by disturbed coal also increases and at the same time, the adsorption constant *a* characterizing the adsorption capacity of coal also increases. The adsorption constant *b* exhibits no clear trend with tectonism, perhaps because changes in pore morphologies due to tectonism are also uncertain.

Data availability statement

The original contributions presented in the study are included in the article/Supplementary Material, further inquiries can be directed to the corresponding authors.

Author contributions

YL: Conceptualization, Writing–original draft, Writing–review and editing. WS: Conceptualization, Writing–original draft, Writing–review and editing. ZW: Conceptualization, Writing–original draft. SM: Writing–original draft. QR: Writing–original draft.

Funding

The author(s) declare financial support was received for the research, authorship, and/or publication of this article. This research was financially supported by the National Key R&D Program of China (Grant No. 2022YFC3004704) and the National Natural Science Foundation of China (Grant No. 52174166), which are gratefully acknowledged.

Conflict of interest

The authors declare that the research was conducted in the absence of any commercial or financial relationships that could be construed as a potential conflict of interest.

Publisher's note

Supplementary material

The Supplementary Material for this article can be found online at: https://www.frontiersin.org/articles/10.3389/fenrg.2024.1333686/full#supplementary-material

References

Agbabiaka, A., Wiltfong, M., and Park, C. (2013). Small angle X-ray scattering technique for the particle size distribution of nonporous nanoparticles. *J. Nanoparticles* 2013, 1–11. doi:10.1155/2013/640436

An, F. H., and Cheng, Y. P. (2014). An explanation of large-scale coal and gas outbursts in underground coal mines: the effect of low-permeability zones on abnormally abundant gas. *Nat. Hazards Earth Syst. Sci.* 14 (8), 2125–2132. doi:10.5194/nhess-14-2125-2014

Cao, D., Wang, A., Ning, S., Li, H., Guo, A., Chen, L., et al. (2020). Coalfield structure and structural controls on coal in China. *Int. J. Coal Sci. Technol.* 7 (2), 220–239. doi:10.1007/s40789-020-00326-z

Chu, P., Xie, H. P., Gao, M. Z., Li, C. B., Shang, D. L., Liu, Q. Q., et al. (2024). Influence of desorption hysteresis effects on coalbed methane migration and production based on dual-porosity medium model incorporating hysteresis pressure. *Comput. Geotechnics* 165, 105893. doi:10.1016/j.compgeo.2023.105893

Dong, J., Cheng, Y., Hu, B., Hao, C., Tu, Q., and Liu, Z. (2018). Experimental study of the mechanical properties of intact and tectonic coal via compression of a single particle. *Powder Technol.* 325, 412–419. doi:10.1016/j.powtec.2017.11.029

Dong, J., Cheng, Y., Jiang, J., and Guo, P. (2020). Effects of tectonism on the pore characteristics and methane diffusion coefficient of coal. *Arabian J. Geosciences* 13 (12), 482. doi:10.1007/s12517-020-05475-8

Dormant, L. M., and Adamson, A. W. (1972). Application of the BET equation to heterogeneous surfaces. *J. Colloid Interface Sci.* 38 (1), 285–289. doi:10.1016/0021-9797(72)90244-5

Ezzati, R. (2020). Derivation of pseudo-first-order, pseudo-second-order and modified pseudo-first-order rate equations from Langmuir and freundlich isotherms for adsorption. *Chem. Eng. J.* 392, 123705. doi:10.1016/j.cej.2019.123705

Fu, X., Qin, Y., Zhang, W., Wei, C., and Zhou, R. (2005). Fractal classification and natural classification of coal pore structure based on migration of coal bed methane. *Chin. Sci. Bull.* 50 (S1), 66–71. doi:10.1007/BF03184085

Han, W., Zhou, G., Gao, D., Zhang, Z., Wei, Z., Wang, H., et al. (2020). Experimental analysis of the pore structure and fractal characteristics of different metamorphic coal based on mercury intrusion-nitrogen adsorption porosimetry. *Powder Technol.* 362, 386–398. doi:10.1016/j.powtec.2019.11.092

Hodot, B. B. (1966). *Outburst of coal and coalbed gas (Chinese Translation)*. Beijing: China Coal Industry Press, 318.

Hou, Q., Li, H., Fan, J., Ju, Y., Wang, T., Li, X., et al. (2012). Structure and coalbed methane occurrence in tectonically deformed coals. *Sci. China Earth Sci.* 55 (11), 1755–1763. doi:10.1007/s11430-012-4493-1

Huang, L., Tan, J., Fu, H., Liu, J., Chen, X., Liao, X., et al. (2023b). The non-plane initiation and propagation mechanism of multiple hydraulic fractures in tight reservoirs considering stress shadow effects. *Eng. Fract. Mech.* 292, 109570. doi:10.1016/j.engfracmech.2023.109570

Huang, L. K., He, R., Yang, Z. Z., Tan, P., Chen, W. H., Li, X. G., et al. (2023a). Exploring hydraulic fracture behavior in glutenite formation with strong heterogeneity and variable lithology based on DEM simulation. *Eng. Fract. Mech.* 278, 109020. doi:10.1016/j.engfracmech.2022.109020

Ji, P. F., Lin, H. F., Kong, X. G., Li, S. G., Cai, Y. C., Wang, R. Z., et al. (2023). Experimental study on enhanced coal seam gas extraction by uniform pressure/pulse pressure N2 injection. *Fuel* 351, 128988. doi:10.1016/j.fuel.2023.128988

Jia, T., Zhang, S., Tang, S., Wang, M., Xin, D., and Zhang, Q. (2022). Characteristics and evolution of low-rank coal pore structure around the first coalification jump: case study in southeastern junggar basin. *Nat. Resour. Res.* 31 (5), 2769–2786. doi:10.1007/s11053-022-10094-z

Jiang, B., Qu, Z., Wang, G. G. X., and Li, M. (2010). Effects of structural deformation on formation of coalbed methane reservoirs in Huaibei coalfield, China. *Int. J. Coal Geol.* 82 (3-4), 175–183. doi:10.1016/j.coal.2009.12.011

Kutchko, B. G., Goodman, A. L., Rosenbaum, E., Natesakhawat, S., and Wagner, K. (2013). Characterization of coal before and after supercritical CO 2 exposure via feature relocation using field-emission scanning electron microscopy. *Fuel* 107, 777–786. doi:10.1016/j.fuel.2013.02.008

Lee, G., Pyun, S., and Rhee, C. (2006). Characterisation of geometric and structural properties of pore surfaces of reactivated microporous carbons based upon image analysis and gas adsorption. *Microporous Mesoporous Mater.* 93 (1-3), 217–225. doi:10.1016/j.micromeso.2006.02.025

Li, W., Jiang, B., and Zhu, Y. (2019). Impact of tectonic deformation on coal methane adsorption capacity. *Adsorpt. Sci. Technol.* 37 (9-10), 698–708. doi:10.1177/0263617419878541

Li, W., Liu, H., and Song, X. (2015). Multifractal analysis of Hg pore size distributions of tectonically deformed coals. *Int. J. Coal Geol.* 144-145, 138–152. doi:10.1016/j.coal.2015.04.011

Lin, H., Bai, Y., Bu, J., Li, S., Yan, M., Zhao, P., et al. (2020). Comprehensive fractal model and pore structural features of medium- and low-rank coal from the zhunnan coalfield of xinjiang, China. *Energies* 13 (1), 7. doi:10.3390/en13010007

Lin, H., Ji, P., Kong, X., Li, S., Long, H., Xiao, T., et al. (2023). Experimental study on the influence of gas pressure on CH4 adsorption-desorption-seepage and deformation characteristics of coal in the whole process under triaxial stress. *Fuel* 333, 126513. doi:10.1016/j.fuel.2022.126513

Liu, L., Yang, M., Cao, Z., and Zhang, X. (2022). Nuclear magnetic resonance study on the law of methane adsorption in water-bearing medium rank lump coal. *Energy Sources. Part a, Recovery, Util. Environ. Eff.* 44 (2), 4411–4426. doi:10.1080/15567036.2022.2077861

Lu, Y., Yang, Z., Li, X., Han, J., and Ji, G. (2015). Problems and methods for optimization of hydraulic fracturing of deep coal beds in China. *Chem. Technol. Fuels Oils* 51 (1), 41–48. doi:10.1007/s10553-015-0573-1

Mangi, H. N., Detian, Y., Hameed, N., Ashraf, U., and Rajper, R. H. (2020). Pore structure characteristics and fractal dimension analysis of low rank coal in the Lower Indus Basin, SE Pakistan. *J. Nat. Gas Sci. Eng.* 77, 103231. doi:10.1016/j.jngse.2020.103231

Meng, Y., and Li, Z. (2018). Experimental comparisons of gas adsorption, sorption induced strain, diffusivity and permeability for low and high rank coals. *Fuel* 234, 914–923. doi:10.1016/j.fuel.2018.07.141

Nie, B., Liu, X., Yang, L., Meng, J., and Li, X. (2015). Pore structure characterization of different rank coals using gas adsorption and scanning electron microscopy. *Fuel* 158, 908–917. doi:10.1016/j.fuel.2015.06.050

Okolo, G. N., Everson, R. C., Neomagus, H. W. J. P., Roberts, M. J., and Sakurovs, R. (2015). Comparing the porosity and surface areas of coal as measured by gas adsorption, mercury intrusion and SAXS techniques. *Fuel* 141, 293–304. doi:10.1016/j.fuel.2014.10.046

Pan, J., Hou, Q., Ju, Y., Bai, H., and Zhao, Y. (2012). Coalbed methane sorption related to coal deformation structures at different temperatures and pressures. *Fuel* 102, 760–765. doi:10.1016/j.fuel.2012.07.023

Qu, Z., Wang, G. G. X., Jiang, B., Rudolph, V., Dou, X., and Li, M. (2010). Experimental study on the porous structure and compressibility of tectonized coals. *Energy and Fuels* 24 (5), 2964–2973. doi:10.1021/ef9015075

Ran, Q., Liang, Y., Zou, Q., Hong, Y., Zhang, B., Liu, H., et al. (2023a). Experimental investigation on mechanical characteristics of red sandstone under graded cyclic loading and its inspirations for stability of overlying strata. *Geomechanics Geophys. Geo-Energy Geo-Resources* 9 (1), 11. doi:10.1007/s40948-023-00555-x

Ran, Q., Liang, Y., Zou, Q., Zhang, B., Li, R., Chen, Z., et al. (2023b). Characteristics of mining-induced fractures under inclined coal seam group multiple mining and implications for gas migration. *Nat. Resour. Res.* 32 (3), 1481–1501. doi:10.1007/s11053-023-10199-z

Ren, J., Niu, Q., Wang, Z., Wang, W., Yuan, W., Weng, H., et al. (2022). CO2 adsorption/desorption, induced deformation behavior, and permeability characteristics of different rank coals: application for CO2 -enhanced coalbed methane recovery. *Energy and Fuels* 36 (11), 5709–5722. doi:10.1021/acs.energyfuels.2c00635

Rigby, S. P. (2005). Predicting surface diffusivities of molecules from equilibrium adsorption isotherms. *Colloids Surfaces a Physicochem. Eng. Aspects* 262 (1-3), 139–149. doi:10.1016/j.colsurfa.2005.04.021

Sun, W., Lin, H., Li, S., Kong, X., Long, H., Yan, M., et al. (2021). Experimental research on adsorption kinetic characteristics of CH4, CO2, and N2 in coal from junggar basin, China, at different temperatures. *Nat. Resour. Res.* 30 (3), 2255–2271. doi:10.1007/s11053-021-09812-w

Sun, Z., Li, L., Wang, F., and Zhou, G. (2020). Desorption characterization of soft and hard coal and its influence on outburst prediction index. *Energy Sources. Part a, Recovery, Util. Environ. Eff.* 42 (22), 2807–2821. doi:10.1080/15567036.2019.1618991

Tan, P., Fu, S. H., Chen, Z. W., and Zhao, Q. (2023). Experimental investigation on fracture growth for integrated hydraulic fracturing in multiple gas bearing formations. *Geoenergy Sci. Eng.* 231 (1), 212316. doi:10.1016/j.geoen.2023.212316

Tan, P., Jin, Y., and Pang, H. W. (2021). Hydraulic fracture vertical propagation behavior in transversely isotropic layered shale formation with transition zone using XFEM-based CZM method. *Eng. Fract. Mech.* 248, 107707. doi:10.1016/j.engfracmech.2021.107707

Ullah, B., Cheng, Y., Wang, L., Yang, W., Jiskani, I. M., and Hu, B. (2022). Experimental analysis of pore structure and fractal characteristics of soft and hard coals with same coalification. *Int. J. Coal Sci. Technol.* 9 (1), 58. doi:10.1007/s40789-022-00530-z

Wang, K., and Du, F. (2020). Coal-gas compound dynamic disasters in China: a review. *Process Saf. Environ. Prot.* 133, 1–17. doi:10.1016/j.psep.2019.10.006

Wang, X., Cheng, Y., Zhang, D., Liu, Z., Wang, Z., and Jiang, Z. (2021). Influence of tectonic evolution on pore structure and fractal characteristics of coal by low pressure gas adsorption. *J. Nat. Gas Sci. Eng.* 87, 103788. doi:10.1016/j.jngse.2020.103788

Wang, Z., Cheng, Y., Qi, Y., Wang, R., Wang, L., and Jiang, J. (2019). Experimental study of pore structure and fractal characteristics of pulverized intact coal and tectonic coal by low temperature nitrogen adsorption. *Powder Technol.* 350, 15–25. doi:10.1016/j.powtec.2019.03.030

Wang, Z., Cheng, Y., Wang, L., Zhou, H., He, X., Yi, M., et al. (2020). Characterization of pore structure and the gas diffusion properties of tectonic and intact coal: implications for lost gas calculation. *Process Saf. Environ. Prot.* 135, 12–21. doi:10.1016/j.psep.2019.12.020

Xu, X., Meng, Z., and Wang, Y. (2019). Experimental comparisons of multiscale pore structures between primary and disturbed coals and their effects on adsorption and seepage of coalbed methane. *J. Petroleum Sci. Eng.* 174, 704–715. doi:10.1016/j.petrol.2018.11.082

Yang, H., Bi, W., Zhang, Y., Yu, J., Yan, J., Lei, D., et al. (2021). Effect of tectonic coal structure on methane adsorption. *J. Environ. Chem. Eng.* 9 (6), 106294. doi:10.1016/j.jece.2021.106294

Yao, Y., Liu, D., Tang, D., Tang, S., and Huang, W. (2008). Fractal characterization of adsorption-pores of coals from North China: an investigation on CH4 adsorption capacity of coals. *Int. J. Coal Geol.* 73 (1), 27–42. doi:10.1016/j.coal.2007.07.003

Ye, C. F., Xie, H. P., Wu, F., and Li, C. B. (2023). Study on the nonlinear time-dependent deformation characteristics and viscoelastic-plastic model of shale under direct shear loading path. *Bull. Eng. Geol. Environ.* 82 (5), 189. doi:10.1007/s10064-023-03170-y

Yu, S., Bo, J., Pei, S., and Jiahao, W. (2018). Matrix compression and multifractal characterization for tectonically deformed coals by Hg porosimetry. *Fuel* 211, 661–675. doi:10.1016/j.fuel.2017.09.070

Zhai, C., Xiang, X., Xu, J., and Wu, S. (2016). The characteristics and main influencing factors affecting coal and gas outbursts in Chinese Pingdingshan mining region. *Nat. Hazards* 82 (1), 507–530. doi:10.1007/s11069-016-2195-2

Zhang, K., Wang, L., Cheng, Y., Li, W., Kan, J., Tu, Q., et al. (2020). Geological control of fold structure on gas occurrence and its implication for coalbed gas outburst: case study in the qinan coal mine, huaibei coalfield, China. *Nat. Resour. Res.* 29 (2), 1375–1395. doi:10.1007/s11053-019-09511-7

Zhao, J. J., Tian, S. X., Li, P., Xie, H. G., and Cai, J. J. (2023a). Molecular dynamics simulation and experimental research on the influence of SiO2-H2O nanofluids on wettability of low-rank coal. *Colloids Surfaces A Physicochem. Eng. Aspects* 679, 132580. doi:10.1016/j.colsurfa.2023.132580

Zhao, J. J., Tian, S. X., Xie, H. G., and Zhang, X. (2023b). Study of time-varying laws of stability and wettability of SiO2–H2O nanofluids with different particle sizes. *Industrial Eng. Chem. Res.* 62 (34), 13529–13540. doi:10.1021/acs.iecr.3c02110

Zhao, P., Liu, H., Li, S., Ho, C., Qin, L., Jia, Y., et al. (2020). Exploring the adsorption and diffusion characteristics of tectonic coal at different mass ratios based on the specific surface Gibbs function. *Powder Technol.* 376, 604–611. doi:10.1016/j.powtec.2020.06.067

Zhao, P., Zhuo, R., Li, S., Lin, H., Shu, C. M., Shuang, H., et al. (2023). Greenhouse gas protection and control based upon the evolution of overburden fractures under coal mining: a review of methods, influencing factors, and techniques. *Energy* 284, 129158. doi:10.1016/j.energy.2023.129158

Zhao, Y., Sun, Y., Liu, S., Wang, K., and Jiang, Y. (2017). Pore structure characterization of coal by NMR cryoporometry. *Fuel* 190, 359–369. doi:10.1016/j.fuel.2016.10.121

Zou, Q. L., Ning, Y. H., Zhang, B. C., Tian, S. X., Jiang, Z. B., and An, Y. Q. (2023a). Mechanical properties and failure characteristics of sandstone under ramp loading paths. *Geomechanics Geophys. Geo-Energy Geo-Resources* 9 (1), 39. doi:10.1007/s40948-023-00574-8

Zou, Q. L., Zhan, J. F., Wang, X., and Huang, Z. (2023b). Influence of nanosized magnesia on the hydration of borehole-sealing cements prepared using different methods. *Int. J. Coal Sci. Technol.* 10, 66. doi:10.1007/s40789-023-00605-5